FULL PAPER

Open Access

Possible correlation between annual gravity change and shallow background seismicity rate at subduction zone by surface load

Yuta Mitsui[*] and Kyohei Yamada

Abstract

The Gravity Recovery and Climate Experiment (GRACE) has monitored global gravity changes since 2002. Gravity changes are considered to represent hydrological water mass movements around the surface of the globe, although fault slip of a large earthquake also causes perturbation of gravity. Since surface water movements are expected to affect earthquake occurrences via elastic surface load or pore-fluid pressure increase, correlation between gravity changes and occurrences of small (not large) earthquakes may reflect the effects of surface water movements. In the present study, we focus on earthquakes smaller than magnitude 7.5 and examine the relation between annual gravity changes and earthquake occurrences at worldwide subduction zones. First, we extract amplitudes of annual gravity changes from GRACE data for land. Next, we estimate background seismicity rates in the epidemic-type aftershock sequence model from shallow seismicity data having magnitudes of over 4.5. Then, we perform correlation analysis of the amplitudes of the annual gravity changes and the shallow background seismicity rates, excluding source areas of large earthquakes, and find moderate positive correlation. It implies that annual water movements can activate shallow earthquakes, although the surface load elastostatic stress changes are on the order of or below 1 kPa, as small as a regional case in a previous study. We speculate that periodic stress perturbation is amplified through nonlinear responses of frictional faults.

Keywords: GRACE, Gravity change, ETAS model, Background seismicity rate, Surface load, Pore pressure

Introduction

Fault slips of earthquakes can perturb the Earth's gravity field (Imanishi et al. 2004; Han et al. 2006), as formulated in elastomechanics (Okubo 1991; Sun and Okubo 1998). Larger earthquakes cause greater perturbation of gravity. Only large earthquakes remain the gravity signals, because of limitation in accuracy of gravity measurement.

By contrast, since gravity changes mainly reflect annually varying shallow water storage as discussed in Hydrology (e.g., Wahr et al. 2004), we expect another relation between earthquakes and gravity changes: some shallow earthquakes may be triggered by water movement around the surface (e.g., Bettinelli et al. 2008; Johnson et al. 2017). In this relation, not only large earthquakes but also small earthquakes should be involved. The physical origins of the earthquake triggering due to water movement around the surface are effects of pore-fluid pressure increase (e.g., Talwani et al. 2007) or elastic surface load (e.g., Heki 2003) on faults.

Nowadays, the Gravity Recovery and Climate Experiment (GRACE) satellites have allowed us to monitor large-scale mass movements. The GRACE satellites investigate 100- to 1000-km-scale gravity changes with an interval of approximately 1 month and can detect great perturbations of gravity due to large (> Mw 8.2) earthquakes (Han et al. 2006; Heki and Matsuo 2010; Han et al. 2013; Tanaka et al. 2015b). However, the relation between gravity changes and small earthquakes that

*Correspondence: mit@shizuoka.ac.jp
Department of Geosciences, Shizuoka University, 836, Ohya, Suruga-ku, Shizuoka 422-8529, Japan

may represent the earthquake triggering mechanisms is not well investigated.

Thus, we examine whether the GRACE gravity changes correlate with occurrences of (small) earthquakes on a global scale. We especially focus on plate subduction zones where earthquakes concentrate.

Materials and methods

Gravity data

We use GRACE level-3 gravity data for land, represented by equivalent water thickness (units: cm), from April 2002 to July 2016, provided by the Physical Oceanography, Distributed Active Archive Center at JPL (Swenson and Wahr 2006; Landerer and Swenson 2012; Swenson 2012). These data were scaled with a worldwide hydrology model in the Global Land Data Assimilation System (Rodell et al. 2004). In particular, we use the GRACE gravity data (analyzed by UTCSR) multiplied by a scaling factor at each spatial grid. Originally, the spatial grid is 1 degree square in latitude and longitude, and a 300-km-wide Gaussian filter to reduce spatial noise is applied. Hence, we spatially average the data every 10 degrees of latitude/longitude only for the grids with finite values (and excluding cases of very few grids), although an actual scale of surface water load may be smaller especially in islands area. The time-series data represent anomalies relative to the 2004.0–2009.999 time–mean baseline. The sampling interval is approximately 1 month. For deficient time-series data, we linearly interpolate the data from the last and the next data. About 10% of the time-series data (18/172) are interpolated.

The temporal gravity change (Δg) with time t (month) at each spatial grid is modeled as

$$\Delta g(t) = A + Bt + C\cos(2\pi t/12) + D\sin(2\pi t/12) \tag{1}$$

where the first term on the right-hand side (A) represents an offset, the second term (Bt) represents a linear trend, and the residual terms represent annual change. Using observation Eq. (1) for the gravity change, we estimate coefficients A, B, C, and D by linear regression using QR decomposition. In the following section, we use the amplitude of the annual gravity change $\sqrt{C^2 + D^2}$. Further, we tried adding terms of semi-annual change to Eq. (1), but the amplitude of the annual change did not almost change.

Earthquake data

In order to evaluate the occurrence of earthquake, we use the ANSS Comprehensive Earthquake Catalogue data from the United States Geological Survey (USGS). We consider only shallow earthquakes at subduction zones, the focal depths of which are shallower than 30 km. Since earthquake occurrences consist of aftershocks (Omori 1894) and other types of background seismicity, we extract the background seismicity rate, μ, using the epidemic-type aftershock sequence (ETAS) model (Ogata 1988).

In the ETAS model, the seismicity rate $\lambda(t)$ at time t is the sum of the background seismicity rate μ and the prior aftershock sequences and is given by

$$\lambda(t) = \mu + \sum_{t_i \le t} \frac{Ke^{\alpha(M_i - M_c)}}{(t - t_i + c)^p} \tag{2}$$

where M_i is the magnitude of the ith earthquake during the observation period, M_c is the minimum earthquake magnitude, and the other parameters (K, c, α, and p) are constants.

In order to estimate the five ETAS parameters in logarithmic form ($\log \mu$, $\log K$, $\log c$, $\log \alpha$, and $\log p$), we adopt two optimization methods for comparison: a limited-memory modification of the quasi-Newton method with box constraints (Byrd et al. 1995) and the differential evolution method (Storn and Price 1997) that is a kind of evolutionary computation to search large spaces of candidate solutions. We assume the initial parameter values (μ, K, c, α, p) = (1, 1, 1, 1, 1) and estimate their optimal values in the ranges of 0.0001–1, 0.1–100, 0.01–10, 0.01–10, and 0.01–10, respectively.

We set $M_c = 4.5$ in order to remove the seismicity of small earthquakes from the Gutenberg–Richter law (Gutenberg and Richter 1944). As a basis for the M_c value, Fig. 1 illustrates the relationship between the number of earthquakes and earthquake magnitudes for the world in the ANSS comprehensive catalogue. The value of $M_c = 4.5$ is the same as that in a previous study estimating the ETAS parameters from the ANSS catalogue (Ide 2013).

The study period to estimate the ETAS parameters is from April 2002 to July 2016, and the spatial range is 10 degrees of latitude/longitude, which is the same as the GRACE data.

We perform correlation analysis for the amplitudes of the annual gravity changes $\sqrt{C^2 + D^2}$ and the background seismicity rate μ. As described in the introduction section, our aim is to clarify the relation between gravity change and occurrence of small earthquakes. Thus, we exclude the areas experienced large earthquakes of magnitude greater than 7.5 in the study period. This deselection is also useful to avoid (aseismic) stressing effects of postseismic deformation within the areas, probably increasing the background seismicity rate μ (Llenos et al. 2009).
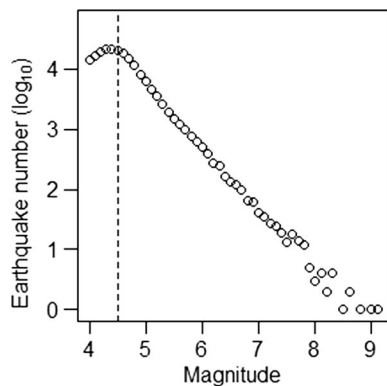
Fig. 1 Earthquake numbers versus magnitudes for the world in the ANSS comprehensive catalogue. The vertical broken line represents magnitude 4.5, which is equal to the threshold value obtained by removing smaller earthquakes from the Gutenberg–Richter law

Results

Figure 2 shows global distribution of the annual gravity change used in this study. We refer to Bird (2003) for locations of plate boundaries. Table 1 shows the results for the amplitude of the annual gravity change.

There are two kinds of the results of the ETAS parameter estimation. One is based on the quasi-Newton method (hereinafter called QN method). In case of this method, we evaluate 95% confidence intervals by calculating inverse of Hessian matrix. The other is based on the differential evolution method (hereinafter called DE method), where we are not able to evaluate confidence intervals. Table 2 exhibits the estimation results of the background seismicity rate μ. We confirm that the results of QN method and DE method are almost the same; therefore, we rely on the estimated values.

Figure 3 compiles the estimated amplitude of the annual gravity change and the background seismicity rate (by QN method). We find a roughly linear relationship between them. The correlation coefficient is 0.51 with a p value of 1.7%. Thus, there is moderate positive correlation between the annual gravity amplitudes and the background seismicity rates. Additionally, we examine correlation between the amplitudes of the annual gravity changes and earthquake numbers (including aftershock effects) in Table 2. In this case, the correlation coefficient is 0.23 with a p value of 31%, which is not a reliable correlation. It is necessary to estimate the background seismicity rate for extracting features of earthquake occurrence without aftershock effects.

Besides, we check a relation between the background seismicity rates and the plate convergence rate (Ide 2013). Figure 4 illustrates our results and the empirical relation proposed by Ide (2013). We find that our results roughly follow the empirical relation but their correlation is not
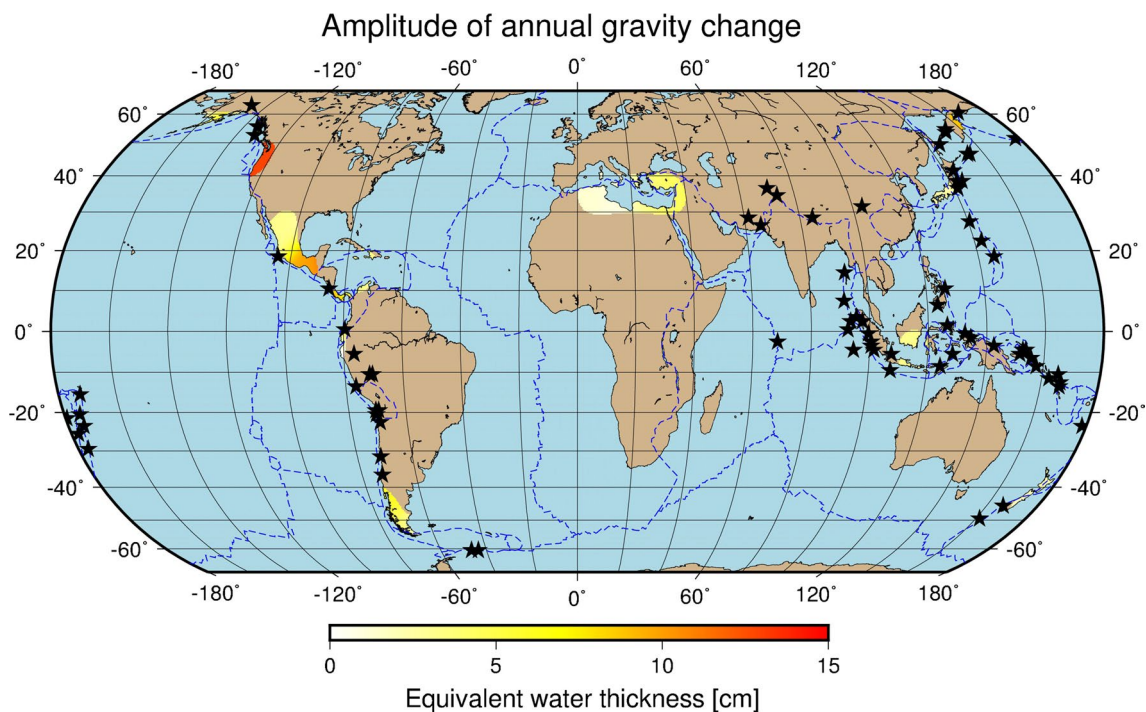

Fig. 2 Distribution of the amplitude of annual gravity change (as equivalent water thickness) in this study. Areas of no data are overlaid with a dark-brown color. Note that we exclude the areas experienced large earthquakes of magnitude greater than 7.5 in the study period. The black stars represent epicenters of the large earthquakes. The blue broken lines show plate boundaries compiled by Bird (2003)

Table 1 Estimated amplitude of the annual gravity change and their 95% confidence intervals, as equivalent water thickness (units: cm), within each spatial area

Long. (°)	Lati. (°)	Annu. grav. (cm)	95% (low) (cm)	95% (up) (cm)
5	35	1.25	0.94	1.57
15	35	0.98	0.62	1.33
25	35	3.12	2.72	3.53
35	35	4.33	3.88	4.78
115	− 5	3.18	2.50	3.86
135	35	2.50	1.84	3.15
165	55	8.71	7.84	9.59
175	− 45	1.81	1.52	2.10
175	− 35	2.45	2.08	2.83
195 (− 165)	55	0.72	0.63	0.81
205 (− 155)	55	5.57	4.96	6.18
215 (− 145)	55	0.55	0.49	0.60
235 (− 125)	45	12.85	11.91	13.79
255 (− 105)	25	3.09	2.67	3.51
265 (− 95)	15	9.84	8.92	10.77
275 (− 85)	− 5	0.45	0.32	0.58
275 (− 85)	5	8.23	7.45	9.00
285 (− 75)	− 55	3.48	2.69	4.28
285 (− 75)	− 45	5.74	5.05	6.43
285 (− 75)	15	3.31	2.97	3.66
295 (− 65)	− 55	1.59	1.18	2.00

The longitude and latitude indicate the center point of each area

strong (correlation coefficient = 0.20). This may be due to the difference of the data set. For example, we did not investigate the areas experienced large earthquakes in the study period, to avoid the effects of postseismic deformation.

Discussion

Examination of effects of pore pressure and surface load

What causes the positive correlation between the annual gravity amplitudes and the background seismicity rates? As described in the introduction section, the relation between gravity change and occurrence of small earthquakes may reflect the earthquake triggering due to water movement around the surface. The possible two mechanisms are friction reduction by pore-fluid pressure increase and elastic stress change due to surface load on faults.

First, we discuss the former effect of pore pressure increase, associated with fluid infiltration from the surface through high-permeability pathway (e.g., fault). This possible triggering effect should be stronger for shallower earthquakes. In order to investigate this point, we vary the depth range of the earthquakes for the correlation study. Our results in the previous section were

based on the earthquakes whose focal depths were shallower than 30 km. We test another threshold value of the depth and check the correlation coefficient between the annual gravity amplitude and the background seismicity rate. Figure 5 shows the results. Unexpectedly, we find that the correlation coefficient does not increase for a smaller threshold value of the depth. We infer that effects of the pore pressure increase hardly trigger the shallow earthquakes.

Next, we examine the latter effect of elastic surface load. As equivalent water thickness, the mass estimated from the GRACE data was on the order of 1–10 cm (Table 1). If we assume that the mass concentrates on the surface for simplicity, we can evaluate hydrostatic pressure of the mass as source of surface load. From the following parameters: 1000 kg/m^3 for water density, 9.8 m/s^2 for gravitational acceleration, and 0.1 m for water thickness, we obtain the hydrostatic pressure about 1 kPa on the surface.

Furthermore, we estimate degrees of Coulomb stress changes (dCFF) on subduction reverse faults due to the surface load, using a two-dimensional Green's function in an elastic half-space (Poulos and Davis 1974). Figure 6 illustrates normalized results of dCFF for left-dipping reverse faults due to unit surface loads. Positive surface loads approximately cause − 0.1 to − 0.7 times stress changes on reverse faults beneath the load area, which should lead to restraining earthquakes. For instance, when the surface load by water mass movement is about 1 kPa as estimated above, the dCFFs on reverse faults are approximately from − 0.1 to − 0.7 kPa. It means that the stress changes on underground faults would be lower than 1 kPa. This value is at least one-order smaller than a typical value of earthquake triggering by elastostatic stress change in the literature (Hardebeck et al. 1998; Freed 2005).

However, not only our study but also a recent study about regional seismicity in California (Johnson et al. 2017) revealed that seasonal water storage, causing stress change on faults as small as 1 kPa, modulated seismicity rates. Recently, on the basis of seismicity analysis (of tremors) about tidal responses, Ide and Tanaka (2014) and Tanaka et al. (2015a) suggested exponential dependence of stress changes on fault slip rates. This corresponds to the rate and state friction framework (Dieterich 1994) based on laboratory rock experiment. Using the rate and state framework, Beeler and Lockner (2003) predicted correlation between earthquake occurrence and periodic stress only in cases of longer periods than earthquake nucleation time. Our result may correspond to their prediction, since the period of the stress changes in our study is annual. Moreover, Tanaka (2014) implied a resonance effect of periodic force on seismicity.

Table 2 Estimated background seismicity rate _µ_ by QN method (with 95% confidence intervals) and by DE method

Long. (°)	Lati. (°)	μ (QN) (day^{-1})	95% (low) (day^{-1})	95% (up) (day^{-1})	μ (DE) (day^{-1})	EQ. number	Conv. rate (cm/year)
5	35	0.0095	0.0068	0.0133	0.0095	80	1
15	35	0.0029	0.0015	0.0054	0.0029	22	1
25	35	0.0282	0.0175	0.0455	0.0288	497	4
35	35	0.0166	0.0133	0.0208	0.0118	84	1
115	− 5	0.0114	0.0058	0.0224	0.0114	111	6
135	35	0.0132	0.0092	0.0189	0.0133	278	5
165	55	0.0121	0.0088	0.0167	0.0122	87	7
175	− 45	0.0126	0.0090	0.0176	0.0127	237	3
175	− 35	0.0072	0.0050	0.0103	0.0072	45	5
195 (− 165)	55	0.0030	0.0018	0.0050	0.0030	16	6
205 (− 155)	55	0.0070	0.0050	0.0099	0.0065	37	6
215 (− 145)	55	0.0004	0.0001	0.0017	0.0004	3	5
235 (− 125)	45	0.0114	0.0082	0.0157	0.0114	83	4
255 (− 105)	25	0.0098	0.0067	0.0143	0.0098	108	2
265 (− 95)	15	0.0337	0.0237	0.0479	0.0337	384	6
275 (− 85)	− 5	0.0049	0.0030	0.0079	0.0049	74	6
275 (− 85)	5	0.0212	0.0165	0.0271	0.0212	180	5
285 (− 75)	− 55	0.0019	0.0010	0.0037	0.0007	11	1
285 (− 75)	− 45	0.0056	0.0028	0.0108	0.0056	65	7
285 (− 75)	15	0.0076	0.0050	0.0116	0.0075	133	1
295 (− 65)	− 55	0.0004	0.0001	0.0017	0.0004	2	1

The longitude and latitude indicate the center point of each area. We also show earthquake numbers and approximated plate convergence rates at each area referring to Bird (2003) and McClusky et al. (2003)
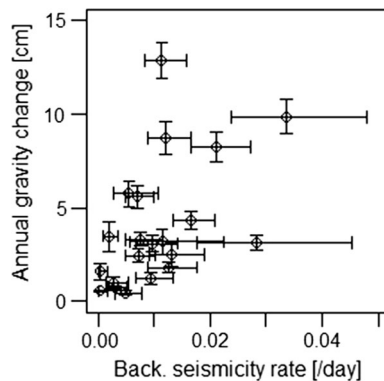

Fig. 3 Amplitude of the annual gravity change versus the background seismicity rate (by QN method). The error bars represent the 95% confidence intervals

Fig. 4 Relation between the estimated background seismicity rates and the plate convergence rates in Table 2. The broken line shows an empirical relation proposed by Ide (2013)

Not clear relation between annual gravity phase and seismicity

We have discussed the possible correlation between the annual gravity "amplitude" and the background seismicity. Here, in the light of "phase" of the annual gravity change, which may reflect the surface load effect on seismicity, we show monthly changes in the gravity as equivalent water thickness and the earthquake number
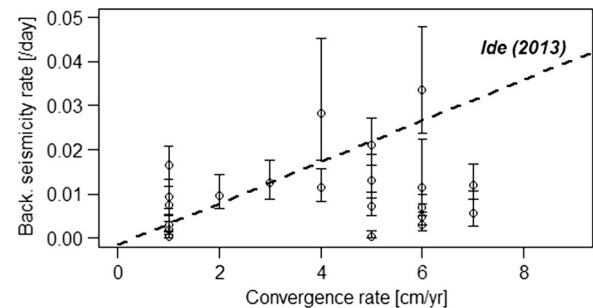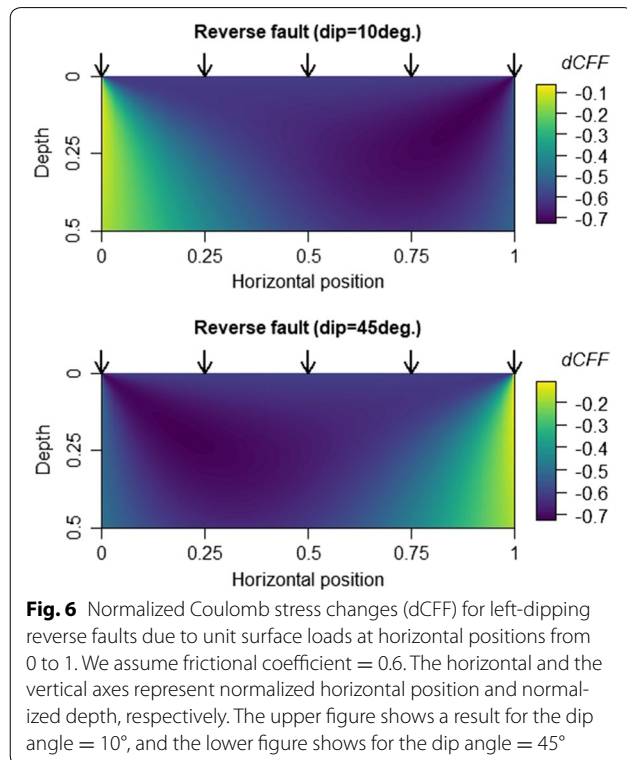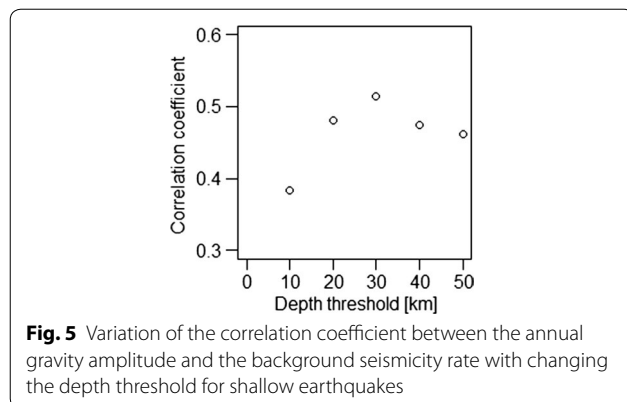
from April 2002, at a grid of (longitude, latitude) = (275°, 5°) and at an adjacent grid of (longitude, latitude) = (275°, − 5°), in Fig. 7. In case of the former grid (Fig. 7a) with a larger amplitude of the annual gravity change, months with many earthquakes tend to be during periods of negative amplitude of the fitted sinusoid. Namely, 6 of 8 months with 5 or more earthquake occurrence, where 5 is a two-sigma threshold of earthquake numbers per month, are in negative amplitude of the fitted sinusoid. The tendency is not apparent in case of the latter grid

Fig. 5 Variation of the correlation coefficient between the annual gravity amplitude and the background seismicity rate with changing the depth threshold for shallow earthquakes

Fig. 6 Normalized Coulomb stress changes (dCFF) for left-dipping reverse faults due to unit surface loads at horizontal positions from 0 to 1. We assume frictional coefficient = 0.6. The horizontal and the vertical axes represent normalized horizontal position and normalized depth, respectively. The upper figure shows a result for the dip angle = 10°, and the lower figure shows for the dip angle = 45°

Fig. 7 Example of monthly changes in the gravity as equivalent water thickness and the earthquake number from April 2002. The black line shows the gravity data, and the red broken line does the fitted curve using Eq. (1). The vertical gray bars represent the earthquake number. The upper figure **a** shows the results at a grid of (longitude, latitude) = (275°, 5°), and the lower **b** shows at an adjacent grid of (longitude, latitude) = (275°, −5°) for comparison

(Fig. 7b) with a smaller amplitude of the annual gravity change. This fact agrees with the negative dependence of the surface loads on the dCFFs, as estimated in the previous paragraph. However, from a statistical point of view, we were not able to reject a null hypothesis under the assumption of random occurrence. At this moment, we state that the relation between the "phase" of the annual gravity changes and seismicity is unclear.

Other possible mechanisms behind the correlation
Our analyses in this study targeted at subduction zones. We have two problems. First, other tectonic factors,
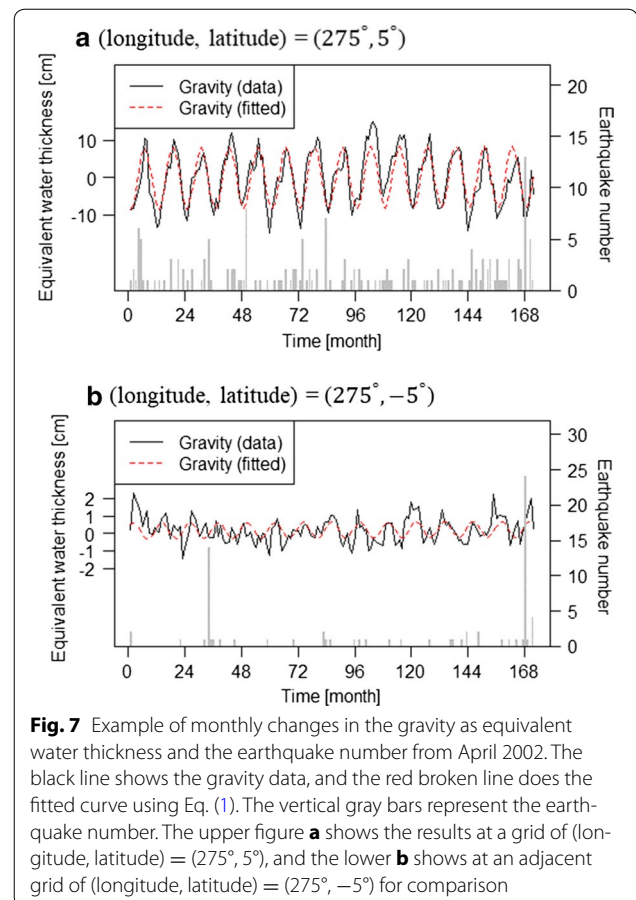
possibly contributing the background seismicity rates (e.g., Nishikawa and Ide 2015), might contaminate the effects of periodic stress perturbation. Thus, inland areas may be more suitable for analyzing the effects of the periodic water mass movements. Since the global seismicity catalogue does not contain sufficient numbers of small (but over M 4.5) inland earthquakes, we did not analyze the inland areas in this study. Second, we did not consider atmospheric and oceanic load effects. Annual changes of atmospheric pressure can be on the order of 1 kPa (Ohtake and Nakahara 1999), comparable to that by the water mass movements in this study. Annual changes of ocean bottom pressure can be also as large as 1 kPa (Tanaka et al. 2015a). These load effects may also modulate seismicities. The above problems would be the focus of our future work.

Conclusions
Through correlation analysis, we find a moderate positive correlation between the amplitudes of the annual gravity changes and the shallow background seismicity rates at the worldwide subduction zones excluding the source areas of large earthquakes. This implies that annual water

cycle can activate shallow earthquakes, although the surface load elastostatic stress changes are on the order of or below 1 kPa, as small as the regional case in the previous study.

Competing interests
The authors declare that they have no competing interests.

Consent for publication
Not applicable.

Ethics approval and consent to participate
Not applicable.

Publisher's Note
Springer Nature remains neutral with regard to jurisdictional claims in published maps and institutional affiliations.

References

Beeler NM, Lockner DA (2003) Why earthquakes correlate weakly with the solid Earth tides: effects of periodic stress on the rate and probability of earthquake occurrence. J Geophys Res 108:2391. https://doi.org/10.1029/2001JB001518

Bettinelli P, Avouac JP, Flouzat M, Bollinger L, Ramillien G, Rajaure S, Sapkota S (2008) Seasonal variations of seismicity and geodetic strain in the Himalaya induced by surface hydrology. Earth Planet Sci Lett 266:332–344. https://doi.org/10.1016/j.epsl.2007.11.021

Bird P (2003) An updated digital model of plate boundaries. Geochem Geophys Geosyst. https://doi.org/10.1029/2001GC000252

Byrd RH, Lu P, Nocedal J, Zhu C (1995) A limited memory algorithm for bound constrained optimization. SIAM J Sci Comput 16:1190–1208. https://doi.org/10.1137/0916069

Dieterich J (1994) A constitutive law for rate of earthquake production and its application to earthquake clustering. J Geophys Res 99:2601–2618. https://doi.org/10.1029/93JB02581

Freed AM (2005) Earthquake triggering by static, dynamic, and postseismic stress transfer. Ann Rev Earth Planet Sci 33:335–367. https://doi.org/10.1146/annurev.earth.33.092203.122505

Gutenberg B, Richter CF (1944) Frequency of earthquakes in California. Bull Seismol Soc Am 34:185–188

Han S-C, Shum CK, Bevis M et al (2006) Crustal dilatation observed by GRACE after the 2004 Sumatra–Andaman earthquake. Science 313:658–662. https://doi.org/10.1126/science.1128661

Han S-C, Riva R, Sauber J, Okal E (2013) Source parameter inversion for recent great earthquakes from a decade-long observation of global gravity fields. J Geophys Res 118:1240–1267. https://doi.org/10.1002/jgrb.50116

Hardebeck JL, Nazareth JJ, Hauksson E (1998) The static stress change triggering model: constraints from two southern California aftershock sequences. J Geophys Res 103:24427–24437. https://doi.org/10.1029/98JB00573

Heki K (2003) Snow load and seasonal variation of earthquake occurrence in Japan. Earth Planet Sci Lett 207:159–164. https://doi.org/10.1016/S0012-821X(02)01148-2

Heki K, Matsuo K (2010) Coseismic gravity changes of the 2010 earthquake in central Chile from satellite gravimetry. Geophys Res Lett 37:L24306. https://doi.org/10.1029/2010GL045335

Ide S (2013) The proportionality between relative plate velocity and seismicity in subduction zones. Nat Geosci 6:780–784. https://doi.org/10.1038/ngeo1901

Ide S, Tanaka Y (2014) Controls on plate motion by oscillating tidal stress: evidence from deep tremors in western Japan. Geophys Res Let 41:3842–3850. https://doi.org/10.1002/2014GL060035

Imanishi Y, Sato T, Higashi T et al (2004) A network of superconducting gravimeters detects submicrogal coseismic gravity changes. Science 306:476–478. https://doi.org/10.1126/science.1101875

Johnson CW, Fu Y, Bürgmann R (2017) Seasonal water storage, stress modulation, and California seismicity. Science 356:1161–1164. https://doi.org/10.1126/science.aak9547

Landerer FW, Swenson SC (2012) Accuracy of scaled GRACE terrestrial water storage estimates. Water Res Res 48:W04531. https://doi.org/10.1029/2011WR011453

Llenos AL, McGuire JJ, Ogata Y (2009) Modeling seismic swarms triggered by aseismic transients. Earth Planet Sci Lett 281:59–69. https://doi.org/10.1016/j.epsl.2009.02.011

McClusky S, Reilinger R, Mahmoud S, Ben Sari D, Tealeb A (2003) GPS constraints on Africa (Nubia) and Arabia plate motions. Geophys J Int 155:126–138. https://doi.org/10.1046/j.1365-246X.2003.02023.x

Nishikawa T, Ide S (2015) Background seismicity rate at subduction zones linked to slab-bending-related hydration. Geophys Res Lett 42:7081–7089. https://doi.org/10.1002/2015GL064578

Ogata Y (1988) Statistical models for earthquake occurrences and residual analysis for point processes. J Am Stat Assoc 83:9–27

Ohtake M, Nakahara H (1999) Seasonality of great earthquake occurrence at the northwestern margin of the Philippine Sea plate. Pure Appl Geophys 155:689–700. https://doi.org/10.1007/s000240050

Okubo S (1991) Potential and gravity changes raised by point dislocations. Geophys J Int 105:573–586. https://doi.org/10.1111/j.1365-246X.1991.tb00797.x

Omori F (1894) On the aftershocks of earthquakes. J Coll Sci Imp Univ Tokyo 7:111–120

Poulos HG, Davis EH (1974) Elastic solutions for soil and rock mechanics. Wiley, New York

Rodell M et al (2004) The global land data assimilation system. Bull Am Meteorol Soc 85:381–394. https://doi.org/10.1175/BAMS-85-3-381

Storn R, Price K (1997) Differential evolution—a simple and efficient heuristic for global optimization over continuous spaces. J Glob Optim 11:341–359. https://doi.org/10.1023/A:1008202821328

Sun W, Okubo S (1998) Surface potential and gravity changes due to internal dislocations in a spherical Earth-II. Application to a finite fault. Geophys J Int 132:79–88. https://doi.org/10.1046/j.1365-246x.1998.00400.x

Swenson SC (2012) GRACE monthly land water mass grids NETCDF RELEASE 5.0. Ver. 5.0. PO.DAAC, CA, USA. https://doi.org/10.5067/TELND-NC005. Dataset accessed 21 Nov 2016

Swenson S, Wahr J (2006) Post-processing removal of correlated errors in GRACE data. Geophys Res Lett 33:L08402. https://doi.org/10.1029/2005GL025285

Talwani P, Chen L, Gahalaut K (2007) Seismogenic permeability, ks. J Geophys Res 112:B07309. https://doi.org/10.1029/2006JB004665

Tanaka Y (2014) An approximately 9-yr-period variation in seismicity and crustal deformation near the Japan Trench and a consideration of its origin. Geophys J Int 196:760–787. https://doi.org/10.1093/gji/ggt424

Tanaka Y, Yabe S, Ide S (2015a) An estimate of tidal and non-tidal modulations of plate subduction speed in the transition zone in the Tokai district. Earth Planets Space 67:141. https://doi.org/10.1186/s40623-015-0311-2

Tanaka Y, Heki K, Matsuo K, Shestakov NV (2015b) Crustal subsidence observed by GRACE after the 2013 Okhotsk deep-focus earthquake. Geophys Res Lett 42:3204–3209. https://doi.org/10.1002/2015GL063838

Wahr J, Swenson S, Zlotnicki V, Velicogna I (2004) Time-variable gravity from GRACE: first results. Geophys Res Lett 31:L11501. https://doi.org/10.1029/2004GL019779

Wessel P, Smith WHF, Scharroo R et al (2013) Generic mapping tools: improved version released. EOS Trans AGU 94:409–410